

Disintegration of Surfactant Micelles at Metal–Water Interfaces Promotes Their Strong Adsorption

Himanshu Singh and Sumit Sharma*

Cite This: *J. Phys. Chem. B* 2020, 124, 2262–2267

Read Online

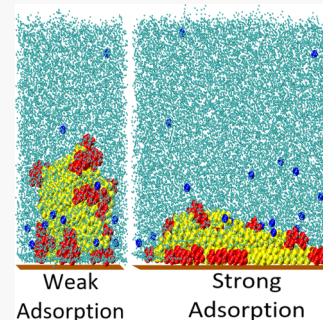
ACCESS |

Metrics & More

Article Recommendations

Supporting Information

ABSTRACT: We have studied the adsorption behavior of micelles of cationic surfactants at metal–water interfaces via fully atomistic simulations. We show that the micelles experience a free energy barrier to adsorption. Near the metal surface, surfactant molecules in the micelles slowly rearrange, leading to complete disintegration of the micelles. The disintegration of the micelles results in much stronger adsorption. After the disintegration, surfactant molecules adsorb by lying flat on the metal surface. Additional simulations performed by treating the micelles as rigid bodies result in only weak adsorption. This confirms our result that disintegration of the micelles is necessary for their strong adsorption.



INTRODUCTION

Surfactant molecules are known to adsorb and self-assemble at the metal–water interfaces in various morphologies.^{1–3} Thus, surfactant adsorption presents a facile way of altering the thermodynamic and transport properties of these interfaces and has been useful in many technological applications, including corrosion inhibition,⁴ modulations of electrochemical reactions,⁵ synthesis of anisotropic metal nanoparticles,⁶ and enhancing specificity in heterogeneous catalysis.⁷ In the bulk aqueous phase, many surfactants exhibit a concentration, known as the critical micelle concentration (CMC), above which they aggregate in micelles. An outstanding as well as an important question is to understand how surfactant micelles adsorb onto surfaces as opposed to unaggregated molecules. This understanding will help in optimizing the concentration and/or composition of surfactants in desired applications. A pertinent example is the use of surfactants as corrosion inhibitors in oil pipelines that span thousands of miles in length: understanding the kinetics of adsorption of unaggregated inhibitor molecules vis-à-vis their micelles will be important for deciding the optimum concentration and composition of corrosion inhibitor mixtures for retarding corrosion.⁸

Atomic force microscopy experiments have revealed that surfactants adsorb on polar surfaces, such as gold, silica, and mica, in various equilibrium morphologies, including cylindrical, spherical, and planar films.^{1,9,10} However, there is lack of clarity on the kinetics of adsorption that are often envisioned simplistically as involving the adsorption of unaggregated molecules, which then self-assemble in ordered configurations.¹¹ Adsorption studies at concentrations above the CMC have reported that surfactant molecules adsorb on polar surfaces with their molecular axes parallel to the surface or as

planar films with the molecules standing up on the surfaces.^{12,13} These studies suggest that surfactant micelles in the bulk phase must be disintegrating upon adsorption. While theory and simulations have elucidated conditions under which different adsorbed morphologies of surfactants on polar surfaces may be observed in equilibrium,^{2,14} the kinetics of adsorption of surfactant micelles remain unclear.

In our previous work, we have shown that unaggregated surfactant molecules adsorb strongly at the metal–water interfaces with no free energy barrier; on the other hand, surfactant micelles experience a free energy barrier to adsorption and are metastable in the adsorbed state.¹⁵ In this work, we show, via molecular dynamics (MD) simulations, that the metastability in the adsorbed state occurs when the micelles do not disintegrate. We report that at relatively long time scales (~ 200 ns), our studied micelles disintegrate near the metal–water interface, and upon disintegration adsorb strongly on the surface. We have performed additional simulations in which the micelles are treated as rigid bodies to show that when the micelles do not disintegrate, they display only a weak adsorption tendency at the metal–water interface. We have studied the micelles of imidazolium-type (henceforth denoted as imid) and quaternary ammonium-type (denoted as quat) cationic surfactants of different alkyl tail lengths. These surfactant types are widely employed as

Received: November 18, 2019

Revised: February 22, 2020

Published: February 24, 2020

inhibitors of internal corrosion in oil and gas pipelines.^{16,17}

Figure 1 shows the chemical structure of these surfactant

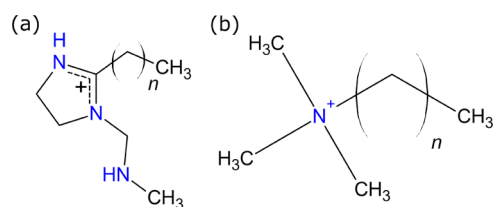


Figure 1. Structure of (a) imidazolium type (imid) and (b) quaternary ammonium type (quat) surfactant molecules employed in this study. The subscript n indicates the length of the alkyl tail. imid-10, imid-17, quat-10, and quat-16 have 10, 17, 10, and 16 carbon atoms in their alkyl tail, respectively.

molecules. The head groups of these molecules carry a positive charge of +1 so as to mimic a pH ~ 5 , typically found in field conditions.

SIMULATION SYSTEM AND METHODS

Our simulation system is comprised of surfactant molecules and counterions in explicit water near a metal lattice. The metal lattice is made of 3588 gold atoms in six layers of face-centered cubic (fcc) lattice in the (111) plane with a lattice constant of 4.08 Å. The simulation box size is 66 Å \times 65 Å \times 145 Å with periodic boundary conditions in the x - and y -directions. The metal lattice is at $z = 0$, and the opposite face of the simulation box has an athermal surface to keep the system volume finite. The top three layers of the lattice close to the aqueous medium are mobile and the bottom three layers are rigid. Water is modeled via the single point charge enhanced (SPC/E) model.¹⁸ The interactions of surfactant molecules are modeled using the general amber force field (GAFF),¹⁹ a popular force field for organic molecules. The total number of water molecules in our system is 15 575. Chlorides are introduced as counterions in the simulation system. The interaction parameters of chlorides are taken from the Joung–Cheatham’s model.²⁰ The interactions of gold atoms are modeled using the interface force field developed by Heinz and co-workers,²¹ which is compatible with GAFF. Partial charges on the surfactant molecules are obtained from density functional theory (DFT). The DFT calculations are performed using Gaussian 09 software by employing B3LYP hybrid functional with 6-31G(d,p) basis set and water as the implicit

solvent.²² A spherical cutoff of 10 Å is chosen for the Lennard-Jones and short-range Coulombic interactions. Long-range Coulombic interactions are computed using the particle–particle particle–mesh (PPPM) method. The simulations are performed in the canonical ensemble at a temperature of 300 K. A vapor space of ~ 20 Å is kept beyond the aqueous medium to maintain the system at a saturation pressure corresponding to $T = 300$ K.²³ Therefore, the overall system is in the isothermal–isobaric ensemble. We have determined the adsorption free energy profiles of the surfactant micelles via umbrella sampling simulations. All MD simulations are performed using large-scale atomic/molecular massively parallel simulator (LAMMPS).²⁴

RESULTS AND DISCUSSION

We have shown previously that both the imid and the quat surfactants aggregate in the bulk phase as spherical micelles, with their polar head groups exposed to water and hydrophobic tails hidden in the core.^{15,25} In unbiased MD simulations, we observed that the surfactant micelles do not adsorb on to the metal surface, indicating presence of an adsorption free energy barrier.¹⁵ In this work, we have calculated the adsorption free energy profiles of different surfactant micelles by performing umbrella sampling²⁶ as a function of the distance of the center of mass of the micelles from the metal surface, ξ . Kindly note that $\xi = 0$ Å corresponds to the location of the center of the topmost layer of gold atoms, that is, the layer exposed to water. Umbrella sampling is performed by keeping a micelle constrained for 80 ns at different locations from the metal surface using a harmonic potential.¹⁵ The first 40 ns run ensures that the system is in equilibrium at each location, which is followed by another 40 ns of production run. A harmonic force constant of 5 kcal/mol/Å² is used to sample the umbrella sampling windows of width 1 Å when the micelles are in the bulk aqueous phase ($\xi > 25$ Å). When close to the metal surface ($\xi < 25$ Å), a larger restraining force is needed. Therefore, we set the force constant to 10 kcal/mol/Å² and the umbrella sampling windows to widths to 0.5 Å. The quality of sampling can be checked by plotting a combined histogram of all the umbrella sampling windows. For some windows at $\xi < 25$ Å, we have performed additional sampling with force constants of 25 and 50 kcal/mol/Å² when the sampling is found to be inadequate in the ξ -space.

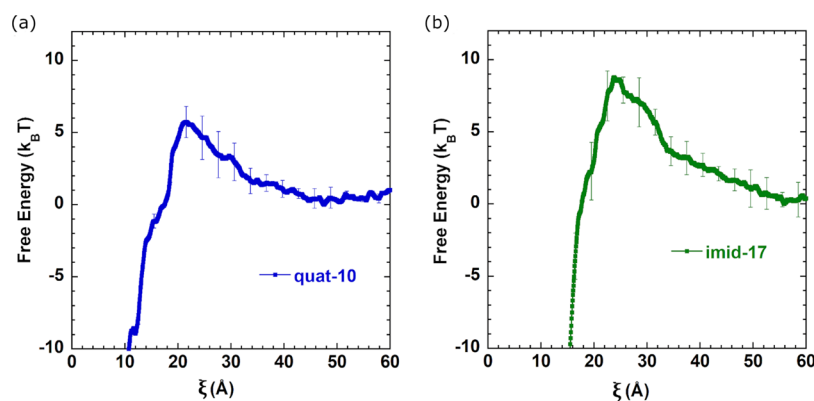


Figure 2. Free energy profiles of the adsorption of quat-10 and imid-17 micelles. Error bars are calculated by generating three independent free energy profiles. The centers of metal atoms in the topmost layer of the metal surface are located at $\xi = 0$ Å.

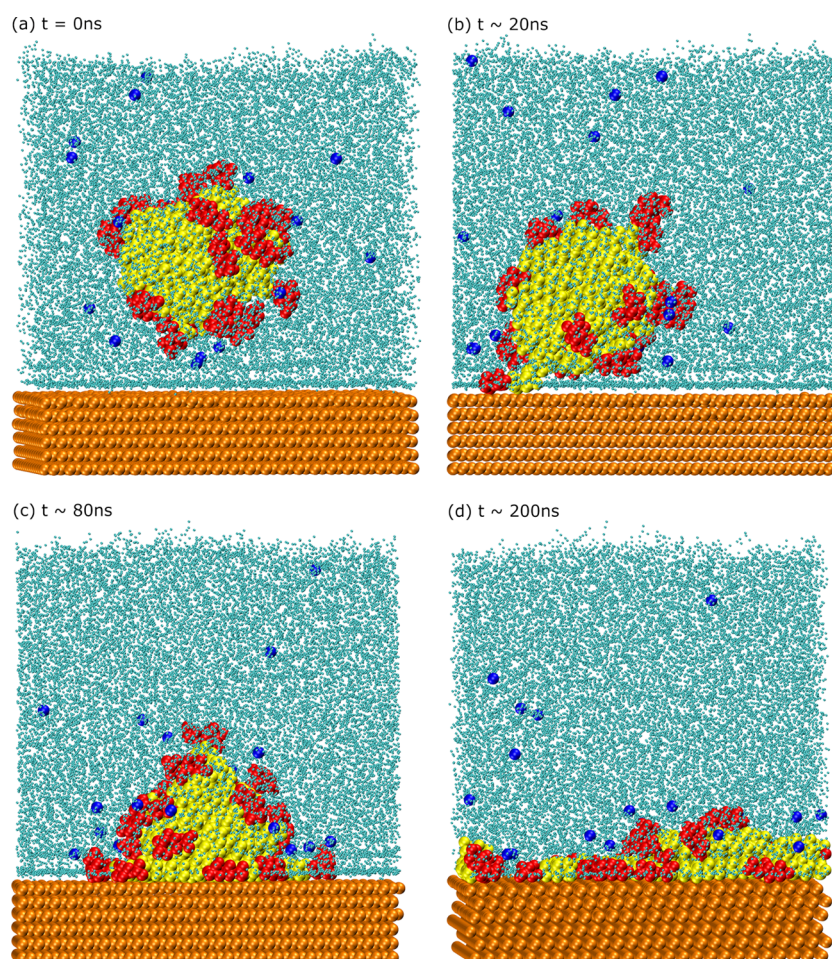


Figure 3. Unbiased MD simulation showing the adsorption and disintegration of imid-17 micelle on the metal surface. Red beads represent the polar head groups and yellow beads represent the alkyl tails of the molecules. Water molecules are shown in cyan color and chlorides are shown in blue color. Orange beads represent the gold lattice.

To form the surfactant micelles, we have performed unbiased MD simulations wherein we randomly insert 60 quat/imid molecules in the bulk aqueous phase in a cubic simulation box of length 65 Å. We find that the quat-10 and the imid-10 molecules in these simulations form the largest micelle comprising of 18 molecules, while the quat-16 and the imid-17 molecules form the largest micelle comprising of 19 molecules.¹⁵ These micelles do not coalesce into larger micelles even after simulated annealing is performed from 400 to 300 K in steps of 10 K. These micelles are used in our adsorption free energy simulations.

Figure 2a,b shows the adsorption free energy profiles of the quat-10 micelle and the imid-17 micelle, respectively. These micelles experience a long-range repulsion of $O(40\text{--}50 \text{ \AA})$ from the metal surface, as has been shown before.¹⁵ Figures S1 and S2 (Supporting Information) show radial distribution functions (RDFs) between the center of mass (COM) of the imid-10 micelle and the chloride ions, and between the chloride ions and the water oxygens, respectively. These RDFs reveal that the corona comprising of solvation water and chloride ions spans a radius of $\sim 30 \text{ \AA}$ from the COM of the micelle. Figure S3 (Supporting Information) shows the density profile of water as a function of the distance from the metal surface, ξ . The layers of adsorbed water span a distance of $\sim 12 \text{ \AA}$ from the metal surface. Therefore, the interaction of the corona of the micelle with the adsorbed water layers results in

the long-range repulsion in the free energy profiles.¹⁵ Once the free energy barrier is crossed, the free energy profile reaches a minimum at the metal surface. We observe that at the metal–water interface, the micelle slowly disintegrates, and the molecules rearrange to maximize their favorable interactions with the surface. In Figure 2, the minimum value in the free energy is plotted only up to $10 k_B T$ to show the features of the profiles clearly. The true minimum of the free energy profile will be a much lower value, estimated as the free energy of adsorption of one molecule multiplied by the number of molecules comprising the micelle. It is noted that the free energy barrier associated with the imid-17 micelle is slightly higher than for the other micelles. This is attributed to the fact that the imidazolium ring is larger than the quaternary ammonium ring. In addition, the imid-17 molecule has a longer alkyl tail than those of the other surfactants studied. As a result, imid-17 micelle is larger in size than other micelles and therefore has more water molecules in its solvation shell (the root mean squared radius of gyration of imid-17 micelle is $11.9 \pm 0.1 \text{ \AA}$, whereas that of quat-10 micelle is $10.8 \pm 0.1 \text{ \AA}$).

To confirm that the surfactant micelles have a natural tendency to disintegrate slowly in the adsorbed state, an unbiased MD simulation is performed by placing the imid-17 micelle at 19 \AA from the metal surface so that it does not need to overcome the free energy barrier at 22 \AA . Snapshots of the micelle near the metal surface at different times is shown in

Figure 3. A movie of this simulation is shown in Movie S1 (Supporting Information).

It is observed in Figure 3 that the micelle first changes shape upon adsorption, wherein the surfactant molecules in the proximity of the metal rearrange to lie parallel to the surface. Over time, more surfactant molecules lie flat on the surface as the micelle disintegrates. Micelles form in the bulk phase primarily due to the hydrophobic effect. Thus, if the free energy of the adsorption of surfactant molecules is more favorable than the free energy of surfactants forming a micelle, then one would expect the micelle to break on the surface. A theoretical model for predicting the criteria for a micelle to break on the surface is provided at the end of the discussion section. A zoomed-in view of the disintegrated imid-17 micelle is shown in Figure 4 to depict the final adsorbed configuration

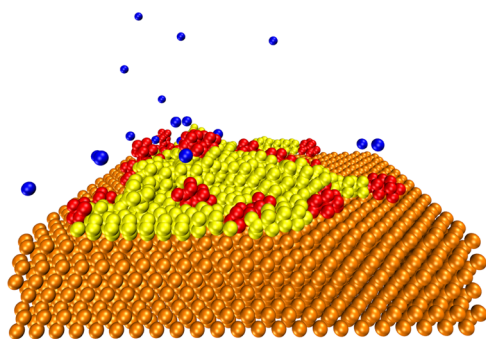


Figure 4. Snapshot of an imid-17 micelle disintegrated on the metal surface. Water molecules are not shown for clarity.

of the micelle after 200 ns. In the most favorable configuration, the molecules tend to adsorb flat on the metal surface. Once adsorbed, the molecules do not detach away because of their strong interaction with the surface. A similar lying-down configuration of quaternary ammonium surfactant molecules on a gold electrode surface, Au(111), has been reported in experiments.²⁷

To bolster our assertion that the strong adsorption is a result of the disintegration of the micelle, we have calculated the adsorption free energies of micelles when they are treated as rigid bodies. A micelle can be treated as a rigid body using the “rigid” command in LAMMPS. The rigid command removes interatomic forces between all atoms that comprise the rigid body, and all external forces and torques are applied to the

center of mass of the rigid body. These rigid micelles cannot deform or rearrange their constituent atoms. Figure 5a,b shows the adsorption profiles of rigid imid-10 and quat-16 micelles along with the nonrigid micelles. To differentiate the rigid micelles from the nonrigid / real micelles discussed previously, we will refer to the latter as nonrigid micelles from now on.

These rigid micelles are created by choosing a micellar configuration that has the asphericity and the squared radius of gyration equal to the average asphericity and the mean squared radius of gyration respectively of the nonrigid micelles in the bulk aqueous phase. The free energy profiles of rigid micelles (Figure 5) show that these micelles experience a long-range repulsion to adsorption similar to those of the nonrigid micelles. However, the rigid micelles do not strongly adsorb on the metal surface, confirming our result that the strong adsorption of nonrigid micelles is attributed to their disintegration. One observation to note is that the peak in the free energy of rigid micelles is larger and closer to the metal surface than that of the nonrigid micelles. In the case of nonrigid micelles, the peak in the free energy profiles is around 22 Å.¹⁵ At smaller distances ($\xi < 22$ Å), the surfactant molecules rearrange within the nonrigid micelle to maximize their favorable interactions with the surface, which results in a decrease in the free energy. However, in the case of rigid micelles, a larger peak at ~ 18 Å is a result of the micelle losing its solvation shell near the metal surface. This loss in energetics because of the disruption of the solvation shell is not compensated by the rearrangement of constituent molecules unlike in the case of nonrigid micelles. The differences in spatial arrangement of constituent molecules in the nonrigid and the rigid imid-10 micelles are clearly observed in Figure S4 (Supporting Information), wherein these micelles are constrained at 17 Å from the metal surface. Figure S5 (Supporting Information) shows the distribution profile of polar head groups of the molecules of the imid-10 micelle at the same location. It is seen in Figure S5 that the surfactant molecules in nonrigid micelles rearrange so that some molecules now lie flat on the surface and so their polar heads are within 3 Å from the metal surface. Note that the free energy profiles of the rigid micelles can only be calculated up to 15.5 Å from the surface since this is the closest distance that these micelles can attain from the metal surface because of their rigidity. A snapshot of an adsorbed configuration of a rigid quat-16 micelle is shown in Figure 6.

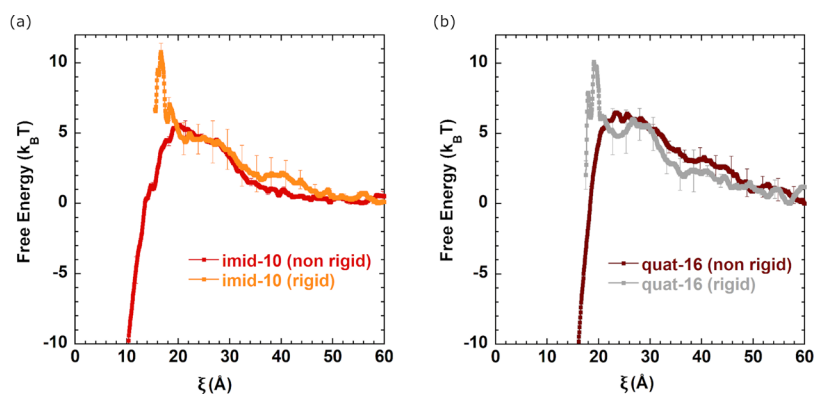


Figure 5. Free energy profiles of the adsorption of rigid and nonrigid micelles of imid-10 and quat-16 molecules. The error bars are determined from three independent free energy profiles.

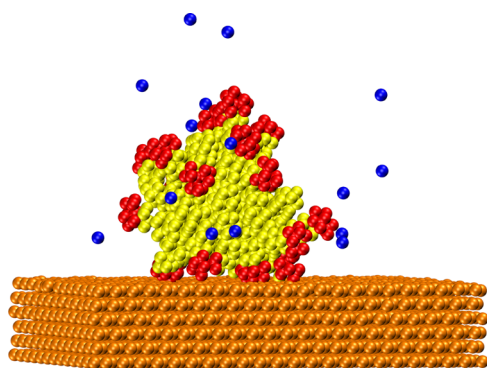


Figure 6. Snapshot of a rigid quat-16 micelle adsorbed on the metal surface. Water molecules are not shown for clarity.

Theoretical Explanation of the Disintegration of Micelles on Polar Surfaces. A surfactant micelle is expected to disintegrate upon adsorption onto a solid–water interface if the free energy of micellization is less favorable than the adsorption free energy of the disintegrated micelle. Let the free energy of micellization be denoted by $\Delta G_{\text{micellization}}$ and the free energy of adsorption of a single surfactant molecule be denoted by Δg_{ads} . Then, the disintegration of the micelle will occur if

$$N\Delta g_{\text{ads}} < \Delta G_{\text{micellization}} \quad (1)$$

where N is the number of surfactant molecules that form the micelle. In our previous studies, we have calculated the Δg_{ads} of individual surfactant molecules at gold–water interfaces and $\Delta G_{\text{micellization}}$ in the bulk aqueous phase.^{15,25} For imid-10 molecule, $\Delta g_{\text{ads}} \approx -30 k_{\text{B}}T$ and $\Delta G_{\text{micellization}}$ (for $N = 18$) $\approx -68 k_{\text{B}}T$. Hence, we find that $N\Delta g_{\text{ads}} \ll \Delta G_{\text{micellization}}$, which suggests that the disintegration of the surfactant micelles is strongly favored at the gold–water interfaces.

CONCLUSIONS

We have studied the adsorption behavior of cationic surfactant micelles at metal–water interfaces using molecular simulations. Our results show that the adsorption behavior of these micelles depends on their structural integrity. In the intact state, the micelles have a weak tendency to adsorb onto the metal surface. However, upon disintegration, the micelles adsorb much more strongly.

ASSOCIATED CONTENT

Supporting Information

The Supporting Information is available free of charge at <https://pubs.acs.org/doi/10.1021/acs.jpbc.9b10780>.

Radial distribution function of chlorides around the center of mass of the imid-10 micelle in the bulk aqueous phase ($\xi = 60 \text{ \AA}$) (Figure S1); radial distribution function (RDF) between water–oxygen and chloride ions at various locations ($\xi = 10, 15, 35, 60 \text{ \AA}$) of the imid-10 micelle from the metal surface (Figure S2); density profile of water as a function of distance from the gold surface (a) in the absence of a micelle, and (b) when the imid-10 micelle is located at different locations ($\xi = 10, 20, 30 \text{ \AA}$) from the metal surface (Figure S3); snapshots showing arrangement of constituent molecules in (a) nonrigid and (b) rigid imid-10 micelles when the micelles are constrained at 17 \AA (free energy peak for rigid micelle) from the metal

surface (Figure S4); distribution of polar head groups of molecules that comprise the rigid and the nonrigid imid-10 micelles when the micelles are constrained at 17 \AA from the metal surface (Figure S5); radial distribution function of water–oxygen around the center of mass (COM) at various locations ($\xi = 10, 15, 20, 60 \text{ \AA}$) of (a) the nonrigid imid-10 micelle and (b) the rigid imid-10 micelle (Figure S6); radial distribution function of chlorides around the protonated nitrogen atoms at different locations ($\xi = 10, 15, 25 \text{ \AA}$) of the imid-10 micelle from the metal surface (Figure S7); angular orientation of a vector joining an atom at the center and an atom on the periphery of the rigid imid-10 micelle with respect to the vector normal to the metal surface¹⁵ (Figure S8) (PDF)

The disintegration of the imid-10 micelle at the gold–water interface. The initial configuration is shown with the micelle at $\sim 15 \text{ \AA}$ from the surface. The movie is captured for 160 ns (Movie S1) (MPG)

AUTHOR INFORMATION

Corresponding Author

Sumit Sharma – Department of Chemical and Biomolecular Engineering, Ohio University, Athens, Ohio 45701, United States; orcid.org/0000-0003-3138-5487; Phone: +1-740-593-1425; Email: sharmas@ohio.edu

Author

Himanshu Singh – Department of Chemical and Biomolecular Engineering, Ohio University, Athens, Ohio 45701, United States

Complete contact information is available at:

<https://pubs.acs.org/10.1021/acs.jpbc.9b10780>

Notes

The authors declare no competing financial interest.

ACKNOWLEDGMENTS

This work is supported by the NSF CBET grant 1705817. The authors thank researchers at the Institute for Corrosion and Multiphase Technology (ICMT) for useful discussions. Computational resources for this work were provided by the Ohio Supercomputer Center and National Science Foundation XSEDE grant number DMR190005.

REFERENCES

- (1) Jaschke, M.; Butt, H.-J.; Gaub, H. E.; Manne, S. Surfactant Aggregates at a Metal Surface. *Langmuir* **1997**, *13*, 1381–1384.
- (2) Ko, X.; Sharma, S. Adsorption and Self-Assembly of Surfactants on Metal–Water Interfaces. *J. Phys. Chem. B* **2017**, *121*, 10364–10370.
- (3) Poirier, G. E.; Pylant, E. D. The Self-Assembly Mechanism of Alkanethiols on Au (111). *Science* **1996**, *272*, 1145–1148.
- (4) Malik, M. A.; Hashim, M. A.; Nabi, F.; Al-Thabaiti, S. A.; Khan, Z. Anti-Corrosion Ability of Surfactants: A Review. *Int. J. Electrochem. Sci.* **2011**, *6*, 1927–1948.
- (5) Franklin, T. C.; Mathew, S. The Use of Surfactants in Electrochemistry. In *Surfactants in Solution*; Springer, 1989; pp 267–286.
- (6) Johnson, C. J.; Dujardin, E.; Davis, S. A.; Murphy, C. J.; Mann, S. Growth and Form of Gold Nanorods Prepared by Seed-Mediated, Surfactant-Directed Synthesis. *J. Mater. Chem.* **2002**, *12*, 1765–1770.
- (7) Thomas, J. M.; Thomas, W. J. *Principles and Practice of Heterogeneous Catalysis*; John Wiley & Sons, 2014.

- (8) Free, M. L. Understanding the Effect of Surfactant Aggregation on Corrosion Inhibition of Mild Steel in Acidic Medium. *Corros. Sci.* **2002**, *44*, 2865–2870.
- (9) Manne, S.; Cleveland, J. P.; Gaub, H. E.; Stucky, G. D.; Hansma, P. K. Direct Visualization of Surfactant Hemimicelles by Force Microscopy of the Electrical Double Layer. *Langmuir* **1994**, *10*, 4409–4413.
- (10) Manne, S.; Gaub, H. E. Molecular Organization of Surfactants at Solid-Liquid Interfaces. *Science* **1995**, *270*, 1480–1482.
- (11) Zhang, R.; Somasundaran, P. Advances in Adsorption of Surfactants and Their Mixtures at Solid/Solution Interfaces. *Adv. Colloid Interface Sci.* **2006**, *123–126*, 213–229.
- (12) Brinck, J.; Jönsson, B.; Tiberg, F. Kinetics of Nonionic Surfactant Adsorption and Desorption at the Silica – Water Interface: One Component. *Langmuir* **1998**, *14*, 1058–1071.
- (13) Xiong, Y.; Brown, B.; Kinsella, B.; Nešić, S.; Pailleret, A. Atomic Force Microscopy Study of the Adsorption of Surfactant Corrosion Inhibitor Films. *Corrosion* **2014**, *70*, 247–260.
- (14) Sharma, S.; Singh, H.; Ko, X. A Quantitatively Accurate Theory to Predict Adsorbed Configurations of Linear Surfactants on Polar Surfaces. *J. Phys. Chem. B* **2019**, *123*, 7464–7470.
- (15) Kurapati, Y.; Sharma, S. Adsorption Free Energies of Imidazolium-Type Surfactants in Infinite Dilution and in Micellar State on Gold Surface. *J. Phys. Chem. B* **2018**, *122*, 5933–5939.
- (16) Cruz, J.; Martinez, R.; Genesca, J.; Garcia-Ochoa, E. Experimental and Theoretical Study of 1-(2-Ethylamino)-2-Methylimidazole as an Inhibitor of Carbon Steel Corrosion in Acid Media. *J. Electroanal. Chem.* **2004**, *566*, 111–121.
- (17) Hegazy, M. A.; Abdallah, M.; Awad, M. K.; Rezk, M. Three Novel Di-Quaternary Ammonium Salts as Corrosion Inhibitors for API X65 Steel Pipeline in Acidic Solution. Part I: Experimental Results. *Corros. Sci.* **2014**, *81*, 54–64.
- (18) Berendsen, H. J. C.; Grigera, J. R.; Straatsma, T. P. The Missing Term in Effective Pair Potentials. *J. Phys. Chem. A.* **1987**, *91*, 6269–6271.
- (19) Wang, J.; Wolf, R. M.; Caldwell, J. W.; Kollman, P. A.; Case, D. A. Development and Testing of a General Amber Force Field. *J. Comput. Chem.* **2004**, *25*, 1157–1174.
- (20) Joung, I. S.; Cheatham, T. E., III Determination of Alkali and Halide Monovalent Ion Parameters for Use in Explicitly Solvated Biomolecular Simulations. *J. Phys. Chem. B* **2008**, *112*, 9020–9041.
- (21) Heinz, H.; Vaia, R. A.; Farmer, B. L.; Naik, R. R. Accurate Simulation of Surfaces and Interfaces of Face-Centered Cubic Metals Using 12–6 and 9–6 Lennard-Jones Potentials. *J. Phys. Chem. C* **2008**, *112*, 17281–17290.
- (22) Frisch, M. J. T. G. W.; Trucks, G. W. S. H. B.; Schlegel, H.; Scuseria, G.; Robb, M.; Cheeseman, J.; Scalmani, G.; Barone, V.; Mennucci, B.; Petersson, G. *Gaussian 09*, Revision, A. 1; Gaussian, Inc.: Wallingford CT, 2009.
- (23) Patel, A. J.; Varilly, P.; Chandler, D. Fluctuations of Water near Extended Hydrophobic and Hydrophilic Surfaces. *J. Phys. Chem. B* **2010**, *114*, 1632–1637.
- (24) Plimpton, S. *Fast Parallel Algorithms for Short-Range Molecular Dynamics*; Sandia National Laboratories: Albuquerque, NM, 1993.
- (25) Singh, H.; Kurapati, Y.; Sharma, S. In *Aggregation and Adsorption Behavior of Organic Corrosion Inhibitors Studied Using Molecular Simulations*, NACE Corrosion Conference, 2019.
- (26) Torrie, G. M.; Valleau, J. P. Nonphysical Sampling Distributions in Monte Carlo Free-Energy Estimation: Umbrella Sampling. *J. Comput. Phys.* **1977**, *23*, 187–199.
- (27) Chen, M.; Burgess, I.; Lipkowski, J. Potential Controlled Surface Aggregation of Surfactants at Electrode Surfaces—A Molecular View. *Surf. Sci.* **2009**, *603*, 1878–1891.